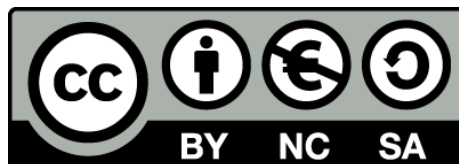# Electric polarization properties of single bacteria measured with electrostatic force microscopy

Theoretical and practical studies of Dielectric constant of single bacteria and smaller elements

Daniel Esteban i Ferrer

UNIVERSITAT DE BARCELONA

Electric polarization properties of single bacteria measured with electrostatic force microscopy

Theoretical and practical studies of Dielectric constant of single bacteria and smaller elements

Daniel Esteban i Ferrer
Barcelona, September 2014

DOCTORAL THESIS

8 Comparison between bacteria and viruses

8.1 Introduction

Applying quantitative EFM methods to very small scale systems has an intrinsic interest. The group has recently published a paper in Nature Materials [29] where we were able to distinguish very small nanoparticles (radius around 10 nm) with similar shape but different material. Also we were able to distinguish DNA-containing viruses from empty ones. From these measurements a label free method to determine the composition of nanoscale objects based on their dielectric response was proposed. The ability to determine the composition of materials at very small length scales is crucial for a wide range of applications, from nanocomposites engineering and characterization [56], [57], [58] to label-free detection for biomedical diagnostics and therapy [59], [60], [61], [62]. Yet it is still a major issue [63], [64], [65], [66], [67] owing to the lack of practical tools with compositional sensitivity at high spatial resolution. But for three-dimensional objects of a few tens of nanometres in size, material identification remains extremely difficult owing to the influence of the exact shape of the tip and of the object on the forces.

An interesting fact to analyze when going from medium size 3D objects to very small scale 3D objects is how the object size affects the modeling of the Electrostatic Force Microscopy measurements. In one hand we have the bacteria, with a height ranging 200 to 700 nm, lengths about 2 μm and widths of around 1 μm. On the other hand small objects like nanoparticles and viruses are as small as 10 nm (radius). Which are the important parameters of the geometry in these small entities? Are there analytical (or approximated) formulas that could be applied? Is the electric field and potential decay in similar or different way?

During the work of thesis I have been analyzing these questions from a modeling point of view. In this chapter a summarize the main conclusions reached for what concerns the modeling of very small scale 3D objects, which complement the study described in this thesis for larger 3D objects like single bacteria. The study includes both homogeneous systems as well as core-shell structures that enables us to distinguish not only the surface but also the inner composition of the objects. Precise numerical calculations based on realistic models of the tip–object system enabled us to account for the geometric effects and to resolve ε_r of dielectric 3D nano-objects with unprecedented selectivity, reliability and resolution.

This chapter reproduces material that appeared in the articles: Fumagalli, L., Esteban Ferrer, D., Cuervo, A., Carrascosa, J. & Gomila, G. (2012). Label-free identification of single dielectric nanoparticles and viruses with ultraweak polarization forces. Nature Materials, 11, 808–816 and Gomila, G., Esteban-Ferrer, D. & Fumagalli, L. (2013). Quantification of the dielectric constant of single non-spherical nanoparticles from polarization forces: eccentricity effects. Nanotechnology, 24(50), 505713. In these two articles I was in charge to build the finite element models and to run and analyze a part of the simulations. This part of the work was performed under the co-supervision of Dra. L. Fumagalli.

8.2 Homogeneous dielectric constant nanoparticle - Phenomenological analytical model vs. numerical simulation of the dielectric signal

To quantify EFM measurements on single dielectric nanoparticles, we need to analyze the electric signals with numerical calculations that take into account the exact geometrical parameters in each experiment and the precise dielectric constant ε_r.
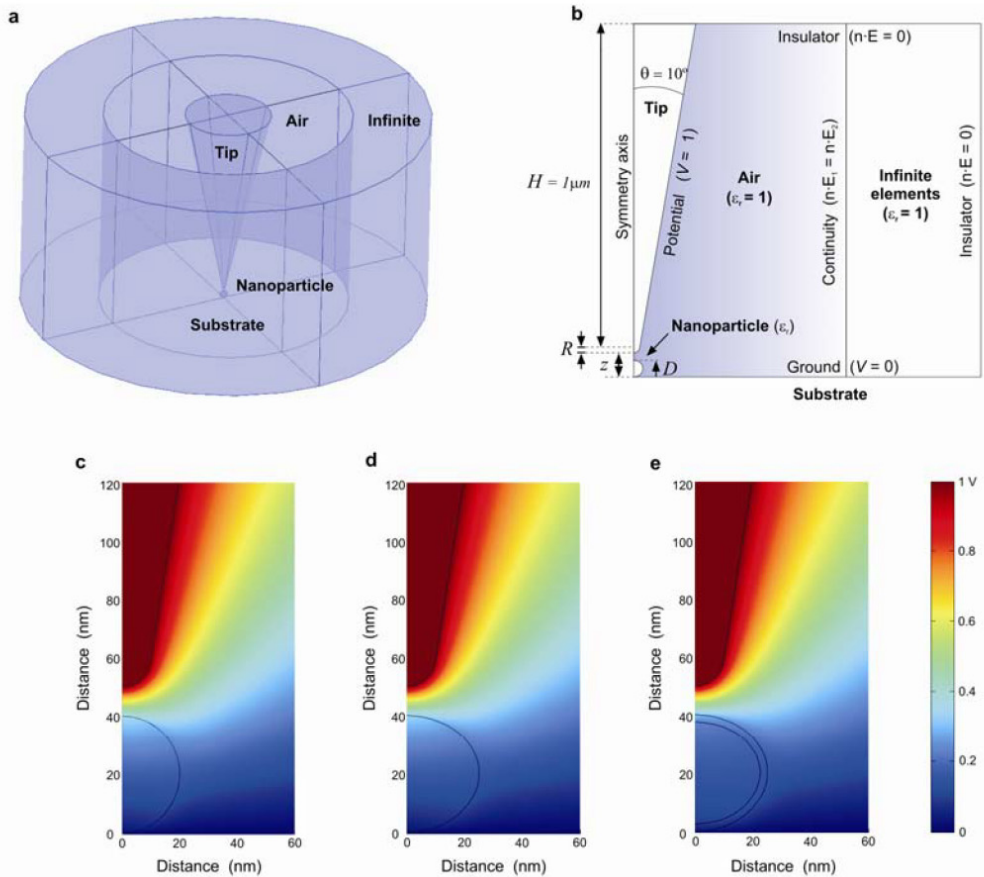
Figure 8.1   (a) 3D simulation box including the tip, the nanoparticle and the substrate, showing the two regions in which the simulation space was divided (air and infinite). (b) 2D axial symmetric representation of the simulation box, indicating the boundary conditions and the parameters of the system. The cone half-angle is 10º and the cone height 1 µm. (c-e) Examples of calculated potential distributions (1V applied) for (c) a spherical nanoparticle (R = 10 nm, D = 40 nm) and a viral particle modeled as an oblate spheroid (R = 10 nm, h = 40 nm, w = 50 nm) of (d) homogeneous material (ε_r = 4) and (e) with a core-shell structure (ε_{core} = 10, ε_{shell} = 2). In (e) the thickness of the shell is 2.5 nm.

We used finite-element calculations (see *Figure 8.1* for geometric and boundary condition details) because an accurate analytical model that exactly reproduces the nanoparticle–tip electrostatic interaction was not available. Spherical, non-spherical and core-shell nanoparticle models were built and investigated.

To understand the influence of ε_r and of the geometrical parameters (R,D,z), we derived from finite-element calculations the following phenomenological model of the dielectric signal at the center of the nanoparticle (maximum) with respect to the substrate

$$\left.\frac{dC}{dz}\right|_{max} - \left.\frac{dC}{dz}\right|_0 = C_0 \frac{(R + r_0)(D - d_0)}{(z - D)^2 + d_1(D - d_2)} log(\varepsilon_r)$$

$$(8.1)$$

where $c_0 \sim 2.22$ zF/nm^{-1} and $r_0 \sim 11.0$ nm are constants, whereas $d_0 = d_0(R) \sim 8\text{-}10$ nm, $d_1 = d_1(R,\varepsilon_r) \sim 2\text{–}3$ nm, $d_2 = d_2(R,\varepsilon_r) \sim 0\text{–}12$ nm are smooth functions of the variables R and ε_r. The explicit expressions of these functions are $\left.\frac{dC}{dz}\right|_{max} - \left.\frac{dC}{dz}\right|_0 = C_0 \frac{(R+r_0)(D-d_0)}{(z-D)^2+d_1(D-d_2)} log(\varepsilon_r)$

$$d_0(R) = d_{00} \frac{1 + \left(\dfrac{R}{r_1}\right)^2}{1 + \dfrac{R}{r_0}}$$

$$(8.2)$$

$$d_1(R, \varepsilon_r) = d_{10} \log\left(\frac{a}{\varepsilon_r}\right)\left[1 + \left(\frac{R}{r_2} - b\log(c\,\varepsilon_r)\right)^2\right]$$

$$(8.3)$$

$$d_2(R, \varepsilon_r) = d_{20}\left(1 - \frac{R}{r_3 \log\left(\frac{d}{\varepsilon_r}\right)}\right)\left(1 + \frac{\varepsilon_r}{e}\right)\log\left(\frac{d}{\varepsilon_r}\right)$$

$$(8.4)$$

In Figure 8.2 we compared the analytical phenomenological model with the numerical calculations. It can be shown that the phenomenological model is accurate within ± 15% with respect to the numerical calculations for the range of tip and nanoparticle size, tip-substrate distance and dielectric constant calculated in the range of parameters: R = 5–30 nm, θ = 10°, D = 20–60 nm, z – D = 10-45 nm and ε_r = 1-10.
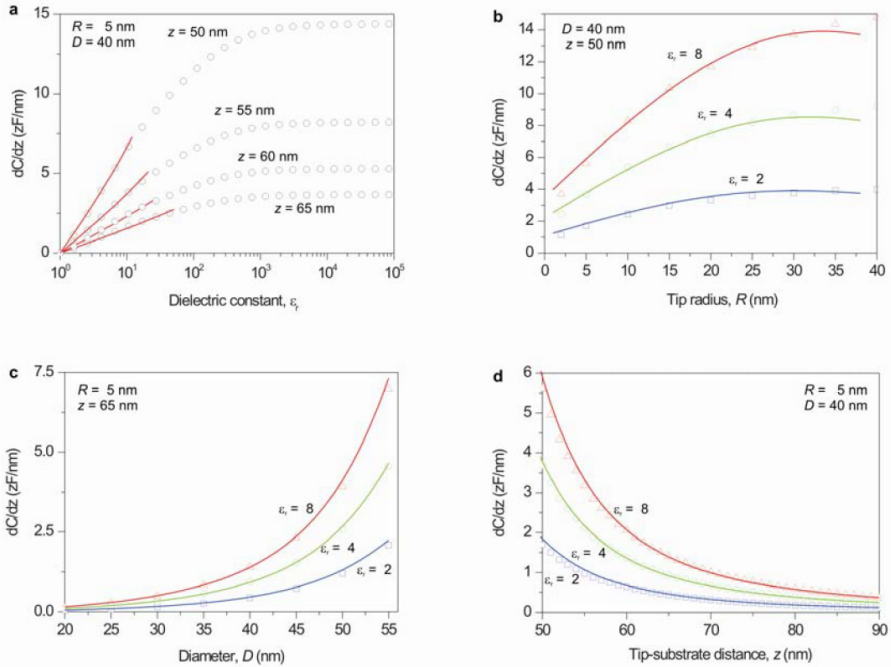
Figure 8.2   Maximal dielectric signal as a function of (a) the dielectric constant, (b) the tip radius, (c) the nanoparticle diameter and (d) the tip-substrate distance. The symbols correspond to finite-element calculations and continuous lines to the analytical equations (8.1)-(8.4). In (a) the different curves correspond to the tip-substrate distances z = 50, 55, 60 and 65 nm (from top to bottom), while in (b) z = 50 nm and in (c) z = 65 nm. In (b-d) the different curves correspond to dielectric constants ε_r = 2 (blue), 4 (green) and 8 (red). Note that in (a) the phenomenological model is only accurate in the range ε_r = 1-10. Geometric parameters when not otherwise stated: R = 5 nm and D = 40 nm.

Note that the phenomenological analytical model of equations *(8.1)*-*(8.4)* is only accurate for dielectric constants in the range of $\varepsilon_r \sim 1$-10. According to equation (8.1) the dielectric signal shows a logarithmic dependence on ε_r for $\varepsilon_r < 10$. This explains the weak dielectric sensitivity to ε_r in front of a much stronger dependence on the geometrical parameters—roughly proportional to R, more complicated on D and with the typical inverse-square power decay with respect to tip–sample distance (z–D).

8.3 Equivalence between the homogeneous and core-shell models of viral particles

The ability of our approach to precisely quantify the dielectric properties and identify materials at the nanoscale was extended to the inner composition of hybrid nano-objects with a core–shell structure. This is because of the long-range nature of polarization forces, which are capable of reaching the material inside the outer shell. We showed it in [28] by measuring and discriminating single viruses—the bacteriophage T7—from their capsids, that is, nanoparticles that have exactly the same shell but different cores. This also illustrates the great potential of this approach to study biological macromolecular complexes, spanning from materials science to biology.

To identify the materials inside the shell, we need to include the internal structure of the nanoparticles into the models. We assumed a core–shell oblate spheroid with dielectric constants ε_{core} for the core and ε_{shell} for the shell. To be specific I consider the case of a virus particle in which the shell thickness is of 2.5 nm. It can be shown that in an external uniform electric field the core–shell model can be made equivalent to the homogenous model described above with an effective dielectric constant given through the equation [49]

$$\varepsilon_{eff} = \varepsilon_{shell} \frac{[(\varepsilon_{core} - \varepsilon_{shell})L + \varepsilon_{shell}] + c(\varepsilon_{core} - \varepsilon_{shell})(1 - L_s)}{[(\varepsilon_{core} - \varepsilon_{shell})L_c + \varepsilon_{shell}] - c(\varepsilon_{core} - \varepsilon_{shell})L_s}$$

(8.5)

where c is the volume fraction of the core, and L_c and L_s are geometrical factors given by

$$L_{ck} = \frac{a_{cx}a_{cy}a_{cz}}{2} \int_0^\infty \frac{dt}{(a_{ck}^2 + 1)\sqrt{(a_{cx}^2 + 1)(a_{cy}^2 + 1)(a_{cz}^2 + 1)}} ; k = x, y, z$$

$$L_{sk} = \frac{a_{sx}a_{sy}a_{sz}}{2} \int_0^\infty \frac{dt}{(a_{sk}^2 + 1)\sqrt{(a_{sx}^2 + 1)(a_{sy}^2 + 1)(a_{sz}^2 + 1)}} ; k = x, y, z$$

The theoretical derivation of equation *(8.5)* is based on the assumption that the electric field at far distances from the spheroid nanoparticle is uniform. In principle, this is not the case for the electric field generated by a sharp tip in close proximity to a spheroid nanoparticle on a metallic substrate, as shown in *Figure 8.3*a, which gives the electric field distribution in our case. In any case we found that the effective dielectric constant obtained from equation *(8.5)* (solid lines), constitutes a very good approximation to the values predicted by finite-element numerical calculations (symbols). In Figure 8.3 we plot the couples of values of ε_{core} and ε_{shell} which give rise to given values of the effective dielectric constant (in the present case that of a virus and a capsid particles).
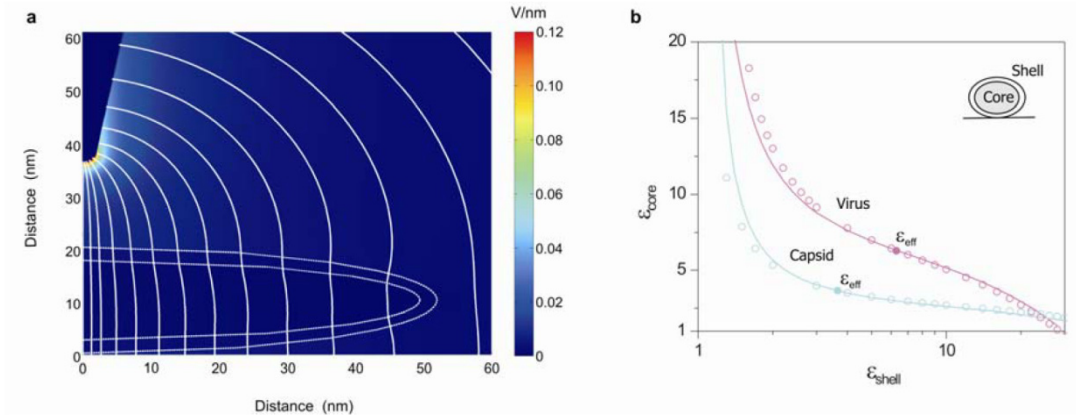
Figure 8.3   (a) Calculated electrostatic field distribution for a tip in close proximity to a dielectric core-shell spheroid nanoparticle on a metallic substrate obtained using finite-element calculations. The color code gives the magnitude of the electric field (V/nm) while the lines give the field lines (the spacing of the lines is in accordance with the magnitude of the electric field). The dielectric constants of the core and shell are ε_{core} = 5 and ε_{shell} = 2, respectively. The applied potential between tip and substrate is 4V, as in the experiments. (b) (Symbols) ε_{core} as a function of ε_{shell} for the virus and capsid in [29] Fig. 4 satisfying the condition that the maximum capacitance gradient calculated by using the core-shell model and finite-element calculations is equal to the measured one (dC/dz = 7.15 and 3.30 zF/nm for the virus and capsid, respectively). (Solid lines) ε_{core} as a function of ε_{shell} for the virus and capsid in [29] Figure 4 satisfying the condition that the effective dielectric constant of the uniform model of equation (8.5) of the paper is equal to the experimentally determined ε_{eff} = 6.30 (virus) and ε_{eff} = 3.65 (capsid). As can be seen, the agreement between the finite element calculations and the analytical model is excellent, thus justifying the use of the analytical model to interpret the measurements. Geometrical parameters correspond to the virus and capsid in [29] Figure 4 (h = 20, w = 104, R = 2 nm and z = 36 nm for the capsid and h = 39, w = 52, R = 5 nm and z = 49 nm for the virus).

The good agreement provided by the analytical formula is probably a consequence of the fact that the portion of the nanoparticle that mostly contributes to the force acting on the tip shows an electric field distribution nearly uniform. Hence, equation *(8.5)* is a good approximation that can be used in quantitative electrostatic force microscopy as an effective uniform model of a core-shell spheroid nanoparticle.

We have verified that this analytical formula cannot be applied to bacteria since the tip radius we use and the height, length and width of the bacteria configures a system where the electrical field is not sufficiently homogeneous as to apply the approximation.

8.4 Quantification of the dielectric constant of single non-spherical nanoparticles from polarization forces: eccentricity effects

We analyze by means of finite-element numerical calculations the polarization force between a sharp conducting tip and a non-spherical uncharged dielectric nanoparticle with the objective of quantifying its dielectric constant from electrostatic force microscopy (EFM) measurements. We show that for an oblate spheroid nanoparticle of given height the strength of the polarization force acting on the tip depends linearly on the eccentricity, e, of the nanoparticle in the small eccentricity and low dielectric constant regimes ($1 < e < 2$ and $1 < \varepsilon_r < 10$), while for higher eccentricities ($e > 2$) the dependence is sub-linear and finally becomes independent of e for very large eccentricities ($e > 30$). These results imply that a precise account of the nanoparticle shape is required to quantify EFM data and obtain the dielectric constants of non-spherical dielectric nanoparticles.
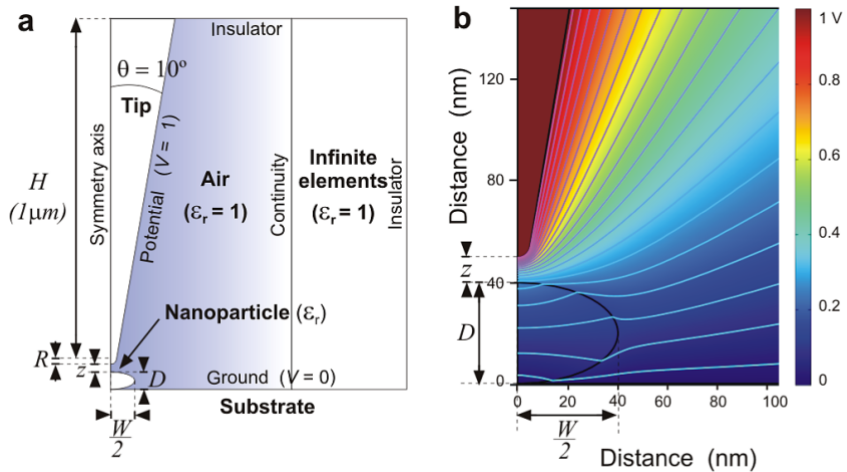
Figure 8.4   (a) Schematic representation of the calculated system and boundary conditions used. (b) Calculated electric potential and equipotential lines (1 V applied) for an oblate spheroidal nanoparticle with eccentricity e = 2 (D = 40 nm, W = 80 nm) and dielectric constant ε_r = 4 polarized with a tip radius R = 5 nm, cone half-angle θ = 10° and cone height H = 1 μm located at z = 10 nm from the nanoparticle.

To perform the study we have considered the tip–nanoparticle system shown schematically in Figure 8.4(a). It consists of a sharp metallic tip, modeled as a truncated cone of height H and cone half-angle θ terminated with a tangent spherical apex of radius R located in close proximity (at a distance z) to a dielectric uncharged nanoparticle with an oblate spheroidal shape, which lies on a conductive substrate. The axial symmetry axis of the tip is assumed to be aligned with the center of the nanoparticle. The nanoparticle has height D, width W and relative dielectric constant ε_r. The eccentricity of the nanoparticle is defined as e = W / D. Thus, for an oblate spheroid nanoparticle one has e > 1. *Figure 8.4*(b) gives an example of an electric potential distribution (1 V applied) calculated for a representative experimental situation of a tip with apex radius R = 5 nm, cone half-angle θ = 10° and an oblate spheroid nanoparticle with height D = 40 nm, width W = 80 nm (e = 2) and dielectric constant ε_r = 4.

In Figure 8.5 shows the variation of the capacitance-gradient contrast, $\Delta C'(z, \varepsilon_r, e)$, as a function of tip–nanoparticle distance, z, for the case of a solid oblate spheroid of dielectric constant ε_r = 6.3, height D = 39 nm and eccentricities e = 1, 2, 5, 10 and 30 (for e > 30 the curves overlap). The tip radius is R = 5 nm. For all eccentricities considered the contrast decays with increasing tip–nanoparticle distance, as expected. In the spherical nanoparticle limit (bottom curve, e = 1) the contrast shows a strong decay with distance, reaching practically zero at a few tens of nanometers (~50 nm) from the nanoparticle. Instead, for larger eccentricities the contrast decays more slowly and it still gives a measurable value at distances larger than 50 nm. We note that for large eccentricities (e > 30) the contrast approaches the one corresponding to an infinitely large dielectric film of the same thickness (and dielectric constant) as the nanoparticle (dashed line in *Figure 8.5*). We then conclude that for small eccentricities (1 < e < 2) the contrast decays with distance in a similar way as it decays for a spherical nanoparticle (a power-law decay), while for large eccentricities the decay is more similar to the one found for a thin dielectric film (a power law plus a logarithmic decay due to the cone contribution, see [38]).

The dependence of the capacitance-gradient contrast on the eccentricity can be better understood by plotting it as a function of the eccentricity at a fixed tip–nanoparticle distance. In Figure 8.5(b) we show it for the same tip–nanoparticle system given in figure 2(a) and for different tip–nanoparticle distances, z = 10, 16, 22 and 30 nm (from top to bottom). We see that for fixed tip geometry, particle height and measuring distance, the dielectric contrast is an increasing function of the lateral diameter of the nanoparticle. For small non-sphericities (1 < e < 2) the increase is roughly linear. This fact can be better appreciated in the inset of Figure 8.5(b), where we plot the capacitance-gradient contrast at a given distance as a function of the eccentricity normalized by the corresponding value obtained for a spherical nanoparticle of diameter equal to the height of the nanoparticle. The curves are linear, showing a slope b = 1–1.4 for the tip–particle distances considered. For larger eccentricities (2 < e < 30) the dielectric contrast increases sub-linearly and saturates to a constant value for very large eccentricities (e > 30).

Finally, in Figure 8.5(c) we show the dependence of the capacitance-gradient contrast on the dielectric constant of the nanoparticle at fixed tip–particle distance (z D 9:5 nm) and different eccentricities in the small eccentricity regime (1 < e < 2, from bottom to top). The dependence on the dielectric constant is qualitatively similar to the one displayed by a spherical nanoparticle (e D 1, bottom line) but it shows larger variations with increasing eccentricity of the nanoparticle. It can be shown that with respect to a spherical particle the contrast increases roughly proportionally to the eccentricity of the nanoparticle for 1 < er < 10.

As a generalization of the formula in equation (8.1) we derived for non- spherical nanoparticles the following equation:

$$\Delta C'_{non-spher}(z, \varepsilon_r, e)$$
$$\approx \left(c_0 \frac{(R + r_0)(D - d_0)}{(z - D)2 + d_1(D - d_2)}\right)\left(1 + b(e - 1)\right)\log(\varepsilon_r)$$

where b = 1–1.4 for 10 nm < z < 30 nm and 1 < ε_r <10.

Results show that even for large radius (R~100) similar to the ones used in bacteria (doped diamond coated tips) the obtained electric forces can be very different if the eccentricity is not properly taken into account. This is something that does not happen in bacteria due to a lager height that makes it only be sensible on the central part (the force density is centered and concentrated on top). See chapter 4.5 for more details. We can also see that formula in ref. [68] is not a good approximation for the probe-sample configuration.

8.5 Conclusions

We can conclude that whereas in the case of small particles (nanoparticles, viruses, etc.) a phenomenological equation could be derived, a similar formula could not be obtained for bacteria since the

geometrical effects and electric field configurations are radically different in both cases.
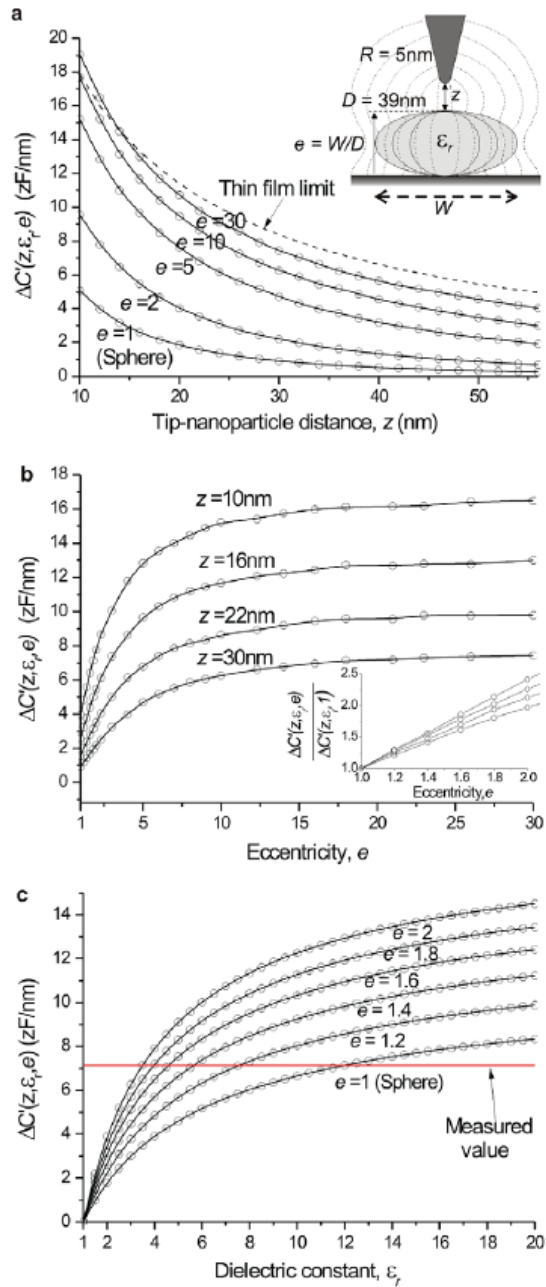
Figure 8.5   Calculated capacitance-gradient contrast at the center of the nanoparticle as a function of the tip–nanoparticle distance for a nanoparticle of fixed dielectric constant ε_r = 6.3 and height D = 39 nm, and different eccentricities e = 1, 2, 5, 10 and 30. Symbols are the calculated points, while continuous lines are interpolated curves. The dashed line corresponds to the case of a large dielectric film of the same thickness and dielectric constant as the nanoparticle. (b) Idem, but as a function of the eccentricity of the nanoparticle for different tip–nanoparticle distances, z = 10, 16, 22, 30 nm. Inset: zoom of (b) in the small eccentricity range (1 < e < 2) normalized by the calculated value for e = 1. (c) Idem, as a function of the dielectric constant of the nanoparticle at fixed tip–nanoparticle distance z = 9.5 nm and different eccentricities in the range 1 < e < 2 (from bottom to top). The horizontal line is the value measured on a single viral particle of spheroidal shape with experimental parameters equal to the ones used in the calculations ($\Delta C'_{virus}$ = 7.15 zF nm^{-1}, see [29]). Tip geometry data: R = 5 nm and θ = 10^0.

Something similar happens with the two shell model, where small objects can be approximated by an analytical formula because the electrical field generated by the probe is approximately homogeneous in the part that mostly contributes to the force, something that does not happen in larger objects like bacteria (in the μm range).

Finally we concluded that for the small objects the eccentricity plays a very important role so the topography has to be precisely measured, whereas in bacteria it is not as important and that is why an axial symmetry of a cone truncated to a tangent sphere over an oblate hemi-spheroid can be used.